International Journal of Pharmaceutics 387 (2010) 272–277

Contents lists available at ScienceDirect

International Journal of Pharmaceutics

journal homepage: www.elsevier.com/locate/ijpharm

Pharmaceutical Nanotechnology

Inclusion of poorly soluble drugs in highly ordered mesoporous silica nanoparticles

M.J.K. Thomas[a], I. Slipper[a], A. Walunj[a], A. Jain[a], M.E. Favretto[b], P. Kallinteri[b], D. Douroumis[a,*]

[a] Medway School of Science, Department of Pharmaceutical Sciences, University of Greenwich, Central Avenue, Chatham Maritime ME4 4TB, Kent, United Kingdom
[b] Medway School of Pharmacy, Universities of Kent/Greenwich, Chatham Maritime ME4 4TB, Kent, United Kingdom

ARTICLE INFO

Article history:
Received 17 September 2009
Received in revised form 7 December 2009
Accepted 9 December 2009
Available online 16 December 2009

Keywords:
Mesoporous silica
SBA-16
Antiepileptic drugs
Loading
Cytotoxicity

ABSTRACT

Silica nanoparticles (MSNs) with a highly ordered mesoporous structures (103 Å) with cubic $Im\bar{3}m$ have been synthesized using triblock copolymers with high poly(alkylene oxide) (EO) segments in acid media. The produced nanoparticles displayed large specific surface area (~765 cm^2/g) with an average particles size of 120 nm. The loading efficiency was assessed by incorporating three major antiepileptic active substances via passive loading and it was found to varying from 17 to 25%. The state of the adsorbed active agents was further analyzed using differential scanning calorimetry (DSC) and X-ray powder diffraction (XRPD). Dissolution studies revealed rapid release profiles within the first 3 h. The viability of 3T3 endothelial cells was not affected in the presence of MSNs indicating negligible cytotoxicity.

1. Introduction

In recent years, mesoporous silica nanoparticles (MSNs) have attracted increasing consideration as a dynamic drug carrier system (Slowing et al., 2008; Liong et al., 2008; Vallet-Regi et al., 2007). These materials were discovered by Mobil scientists (Kresge et al., 1992; Beck et al., 1992) know as MCM-41 or MCM-48 and used as molecular sieves. It was firstly Vallet-Regi et al. (2001) who proposed the use of MSNs as drug delivery system by loading ibuprofen into the mesoporous MCM-41 material. MSNs possess several features that render them excellent candidates as drug delivery systems such as the ordered pore network, with very homogeneous size that controls the drug load and release kinetics. In addition the high pore volume and the high surface area facilitate the adsorption of high active substances amounts. By adjusting also the pore size slightly larger than the dimension of the drug molecule MSNs can serve as a versatile host of various substances. Finally, the silanol-containing surface can be functionalized to induce better control over drug loading and release properties.

MSNs are synthesized though either the alkaline route (Beck et al., 1992) or the acid route (Huo et al., 1994) both using amphiphiles as templates. The acid catalysis accelerates the hydrolysis versus the condensation rate and promotes mainly condensation at the ends of silica polymers to form linear silicate ions. On the other hand, the alkaline catalysis favors both hydrolysis and condensation. Two main synthetic pathways have been proposed so far to enlighten the formation of the mesoporous structure. The first one, known as the "liquid-crystal template mechanism", suggests that the hexagonal, liquid-crystal surfactant phase exists in the solution prior the addition of the silica precursors. The silica framework precipitates around this template, forming a mesoporous structure. The surfactants are then removed by calcination, thus creating a porous structure with a high surface area. In the latter, the surfactants are aggregated as single, rod-like micelles before the addition of the silica precursors. The addition of silica enables these species to interact with the surface of the surfactant micelles, which sets off the surfactant rods to assemble into a hexagonal array.

Administration of MSNs can take place through parenteral and oral route. One of the main advantages is the ability to increase the solubility of poorly water soluble drugs while they can also be used for hydrophilic active agents. Thus high drug loading can be achieved with loading capacities normally varying from 10 to 34% (Qu et al., 2006) or up to 60% in extreme cases (Heikkilä et al., 2007). They have been also used for controlled release and drug targeting providing sustained release for 16 h (Wen et al., 2006).

Carbamazepine (CBZ), oxcarbazepine (OXC) and rufinamide (RFN) are three major antiepileptic drugs classified by the Biopharmaceutics Classification System (BCS) as Class II active pharmaceutical ingredients (Amidon et al., 1995; Amidon and Löbenberg, 2000) because they present low solubility and high permeability. They are poorly water soluble drugs and the dissolution is the rate-limiting factor for absorption. Thus it is important to

* Corresponding author. Tel.: +44 0208 8331 8440; fax: +44 0208 8331 9805.
E-mail address: D.Douroumis@gre.ac.uk (D. Douroumis).

0378-5173/$ – see front matter © 2009 Elsevier B.V. All rights reserved.
doi:10.1016/j.ijpharm.2009.12.023

increase drug solubility resulting to absorption and bioavailability enhancement. All active agents are broad-spectrum anticonvulsants used in the treatment of inadequately controlled partial seizures in adult patients and in seizures associated with Lennox-Gastaut syndrome. Currently, the existing commercial products of CBZ and OXC are under the trade names Tegretol® and Trileptal®, respectively while RFN is in phase III clinical trials.

The available nanoparticulate drug delivery systems include a large number of inorganic and organic materials among them liposomes (Schiffelers and Storm, 2008), micelles (Blanco et al., 2009), polymeric nanoparticles (Lin et al., 2009), quantum dots (Delehanty et al., 2009), gold nanoparticles (Sperling et al., 2008), and magnetic nanoparticles (Polyak and Friedman, 2009). Each of these systems has gained interest among the researchers as a potential mean to formulate and deliver active molecules. Nevertheless, there is a lack of nanoparticulate formulations of the aforementioned active agents and only two studies (Douroumis and Fahr, 2006, 2007) from our group have been reported to the literature up to date. The main obstacle to overcome is the particle size stability of the produced nano-colloidal systems due to rapid recrystallization by spontaneous nucleation. This can lead to premature release of the active substance from the carrier altering the physicochemical properties of the developed formulation.

In the current study we synthesized highly ordered mesoporous silica nanoparticles with cubic symmetry using triblock non-anionic surfactants. Due to the increased surface area MSNs display structural properties required for drug carriers. The drug loading capacity of the synthesized nanoparticles was assessed using the above active agents as model substances. In general, MSNs are biocompatible and do not present long term side effects (Kortesuo et al., 1999) when used as implants. Due to the limited number of such reports we also investigated MSNs' cytotoxicity by assessing the viability of 3T3 endothelial cells.

2. Materials

2.1. Materials

Tetraethyl orthosilicate (TEOS) was obtained from Sigma Aldrich (St. Lewis, USA). The active agents carbamazepine, oxcarbazepine and rufinamide were kindly donated from Novartis Pharma A.G. (Basel, Switzerland). Poloxamer F127 was donated from BASF GmbH (Ludwigshafen, Germany). The HPLC grade solvents dimethylformamide (DMF), ethanol, chloroform and acetonitrile were purchased from Fisher Chemicals (Karlsruhe, UK). All materials were used as received.

2.2. Synthesis of mesoporous silica nanoparticles

Silica-block copolymer mesophases were synthesized using Pluronic F127 as a structure reacting agent which was reacted at room temperature. In a routine preparation, 4.0 g of Pluronic P127 was dissolved in 30 g of water and 120 g of 2 M HCl solution with constant stirring at 25 °C. Then 8.50 g of TEOS was added into that solution with stirring at 35 °C for 20 h. The mixture was aged at 80 °C overnight without stirring. The solid product was recovered, washed, and air-dried at RT. Calcination was carried out by slowly increasing temperature from room temperature to 500 °C in 8 h and heating at 500 °C for 6 h. For the removal of F127 the solid product was also washed with copious amounts of ethanol and water after low temperature reflux in ethanol.

2.3. Loading of active agents

The passive method was used to load SBA-16 nanoparticles with the three active agents (Fig. 1 depicts the molecular structure). Two different organic solvents were used for the loading process depending on the drug solubility. For CBZ, 0.1 g of SBA-16 were added in 1.0 ml CBZ methanolic solution of concentration Co (Co = 100 mg/ml). The adsorption procedure was carried out overnight under gentle stirring. Subsequently, the suspensions were filtered (MF^{TM} membrane filters, pore size 0.05 μm, Millipore) and CBZ that remained in the filtrate was further determined using HPLC. The same process was repeated for OXC and RFN by using dimethylformamide (DMF) solutions of 40 mg/ml, respectively, due to the low solubility of both active agents in organic solvents.

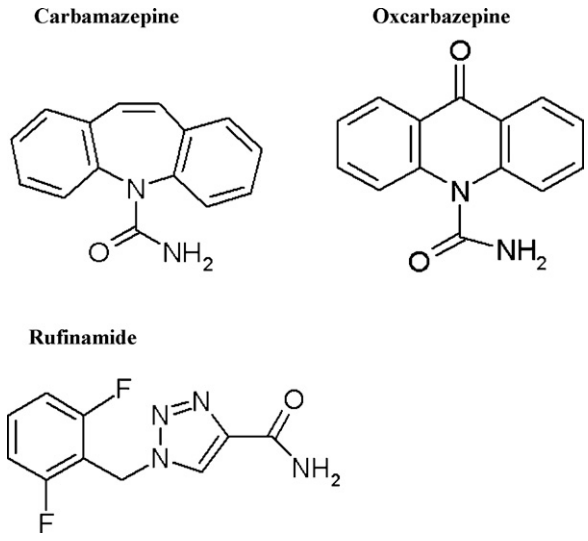

Fig. 1. Molecular structures of carbamazepine, oxcarbazepine and rufinamide.

2.4. Determination of loading efficiency

The loading efficiency of SBA-16 nanoparticles was determined by adding 50 mg of loaded samples in 20 ml ACN and stirred for 24 h. The samples were centrifuged in a Sorval RC6 Plus centrifuge at 7000 rpm for 30 min. The supernatant was collected and determined with HPLC analysis.

2.5. Particle size measurements

The particle size of the dispersions was measured with Malvern Masterisizer 2000 (Malvern, UK) combining information from simple light scattering (LS) and polarization intensity differential scattering (PIDS). For data evaluation, an optical model based on the Mie theory was created using the instrumental software assuming 1.45 as the real and 0 as the imaginary part of the refractive index of the particles. Results given are the mean of 5 successive measurements of 120 s each.

2.6. Scanning electron microscopy

The morphology of newly synthesized MSNs was examined by scanning electron microscopy (SEM). The samples were attached to aluminum stubs with double side adhesive carbon tape then gold coated and examined using a scanning electron microscope (Jeol 5200, SEM).

2.7. Differential scanning calorimetry

The physical state of the pure drugs and the loaded MSNs samples were examined by differential scanning calorimetry (DSC). The thermographs of each powder were obtained by using a Mettler Toledo 823e (Greifensee, Switzerland) differential scanning

calorimeter. Samples accurately weighted (2–3 mg) were placed in pierced aluminium pans and heated from 20 to 260 °C at a scanning rate of 10 °C min^{-1} in a nitrogen atmosphere.

2.8. Powder X-ray diffraction

Samples of MSNs were evaluated using a Kristalloflex 810 Siemens diffractometer. The samples were radiated using Ni filtered CuKα radiation operated at 40 kV and 30 mA. The MSNs samples were scanned from 0.7 to 5 of diffraction angle (2θ) at scanning speed of 0.02 2θ/s.

2.9. BET analysis

BET surface area, pore volume and pore diameter of SBA-16 mesoporous material was measured by using Micromeritics Gemini 6 (Norcross, USA) automated gas sorption system model. The determination of micropore volume, micropore surface area, and external surface area was estimated by using the standard t-plot calculations, while the pore size and distribution was estimated using Broekhoff and de Boer (BdB) reports.

2.10. Dissolution studies

The release of the SBA-16 loaded samples was studied by using a USP/Ph.Eur. paddle dissolution apparatus (Varian 705 DS, Weston, USA). All release studies were carried out under sink conditions in triplicate. The powders were added to 900 ml phosphate buffer solution (pH 7.4) at 37 °C and the paddle speed was set to 100 rpm. At predetermined sampling times 5 ml aliquots were taken and filtered through a 0.1-μm filter. The removed fluid was instantly replaced with an equal amount of fresh dissolution medium. The dissolution studies carried out for 24 h.

2.11. HPLC analysis

The concentration of drug in the samples was determined by HPLC. An Agilent 1200 Series (Waldbronn, Germany) equipped with a multiple wavelength detector (MWD) and a Beckman-Coulter Nucleosil 100 RP, 5 μm × 4.5 mm × 25 cm column was used for HPLC assay. Mobile phase contained ACN/water/phosphoric acid at a ratio of 49.9:49.9:0.2 (v/v/v). Mobile phases were left to stand for at least 12 h. The flow rate was 1.0 ml min^{-1} and the injection volume was 20 μL while column temperature maintained at 25 °C. The wavelength was monitored at 236, 254 and 261 nm for CBZ, OXC and RFN, respectively. Calibration curves were constructed using standard solutions of known concentrations from 5 to 50 μg/ml. The Agilent software calculated the peak area of each standard solution and sample automatically.

2.12. Cell culture and cytotoxicity studies

3T3 cell line was kindly donated by Dr. T. Parker (Biomedical Sciences, University of Nottingham). Cells were cultured in DMEM medium containing 10% FBS and incubated at 37 °C in 5% CO_2 humidified incubator.

Viability of rodent fibroblasts (3T3) was evaluated using MTT assay, which is associated to cell mitochondrial activity. The assay is based on the ability of viable cells to convert thiazolyl blue tetrazolium bromide solution to the blue formazan crystals in their mitochondria (Mosmann, 1983). Briefly, the cells were seeded at a concentration of 5×10^4 cells/ml/well in 24-well plates and were incubated with silica nanoparticles at increasing concentrations for 1 day. The cells in the first three wells were incubated in the absence of the formulation. DMSO (0.5 ml/well) was used as positive control for cell death. After 24 h of incubation, 100 μL of MTT solution (concentration 5 mg/ml) was added to the wells and incubated for 2 h at 37 °C. The blue formazan salts were dissolved in 100 μL of acidified isopropanol (0.33 μL HCl in 100 ml isopropanol), which was transferred to 96-well plates and the absorbance was read on a microplate reader (Bio-Tec Instruments) at wavelength of 490 nm. Cell viability was calculated by comparing the number of viable cells in the formulation-treated wells to the non-formulation treated cells.

All data were reported as the mean ± standard deviation (SD). Statistical analysis was performed for the experiments conducted in triplicate using Student's *t*-test. Results with $p < 0.05$ were considered to be statistically significant.

3. Results

3.1. Silica synthesis and characterization

MSNs were prepared trough the sol–gel process using a poly(alkylene oxide) triblock copolymer, $EO_{101}PO_{56}EO_{101}$ as structure directing agent (Zhao et al., 1998). The process carried out in acid media below the isoelectric point of silica where the silica precursors will be present as cationic species. The process described by Zhao et al. (1998) leads to intermediate mesophases through a $(S^0H^+)(X^-I^+)$ route where S^0 is the surfactant, X^- is the halide anion, and I^+ is a protonated Si–OH moiety. Initially alkoxysilane species hydrolyzed and the surfactant EO parts interact with hydronium ions. The cationic silanol groups interact with the charged EO groups through a combination of electrostatic, hydrogen bonding and van der Waals interactions. Hydrolysis and condensation of the silica species continue until the lowest energy silica-surfactant mesophase structure is formed by solidification of the inorganic structure.

By altering the percentage of F127 (1–6%) we were able to manipulate the surface area, the pore volume and the pore size (not shown). The produced nanoparticles displayed uniform and narrow particle size distribution of approximately 120 nm as it is depicted in Fig. 2. Zeta potential measurements gave values of −7.8 mV. The estimated BET specific surface area was 765 $m^2\ g^{-1}$, with a measured mesoporous volume of 0.61 $cm^3\ g^{-1}$ and a narrow pore size distribution of 35 nm. The obtained value for this pore wall thickness is 0.34 nm. In Fig. 3, the BET isotherm is depicted and also the pore size distribution in the inset figure obtained by the Broekhoff and de Boer (BdB) method. As it can be seen it is a characteristic type IV isotherm of mesoporous materials with a step in the range of $P/P_0 = 0.40–0.65$ which is typical for the filling of standard mesoporous systems. The thickness (h) of the pore wall can be estimated by using the pore volume data (porosity) based on the following equation (Ravikovitch and Neimark, 2000):

$$h = \frac{2}{\rho_s S} \quad (1)$$

where ρ_s is the true density of solid obtained from helium pycnometer and S the estimated specific surface area. Using the above equation the mean pore wall thickness was found to be 11.8 Å.

In Fig. 4, the XRD pattern of calcinated SBA-16 shows a strong reflection with a large d spacing of 103 Å two strong reflections in the 2θ range of 1–1.4° with d spacings of 72.68 and 59.47 Å, respectively. The Miller indices of the XRD pattern of SBA-16 have the (1 1 0), (2 0 0), (2 1 1) reflections corresponding to a cubic structure $Im\bar{3}m$ with a large cell parameter, $a = 166$ Å, for the calcined SBA-16 material.

The above studies demonstrate that the SBA-16 silica nanoparticles used for this investigation exhibit a well-ordered 3D mesoporous structure.

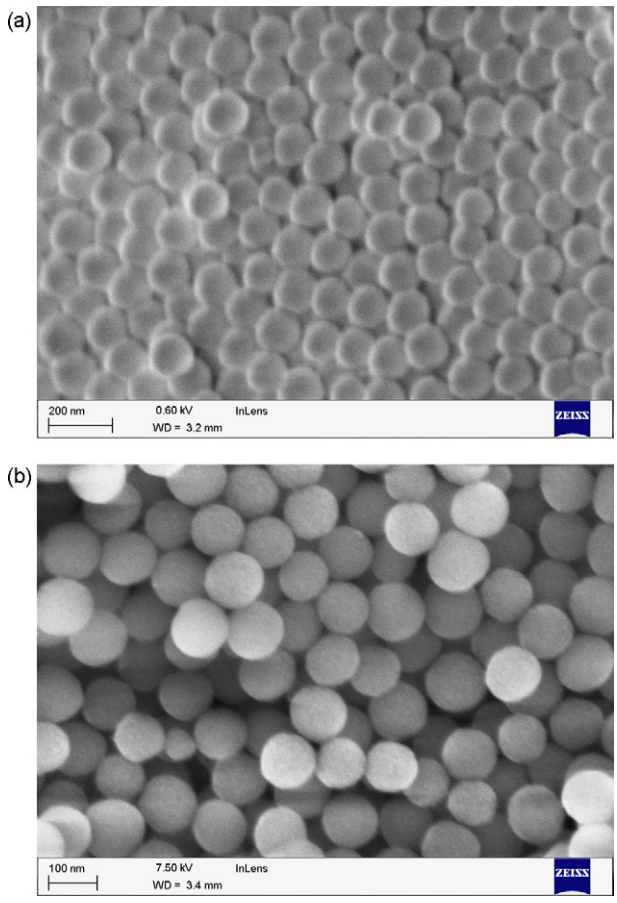

Fig. 2. SEM micrographs of SBA-16 nanoparticles.

3.2. Drug inclusion into SBA-16

One of the main objectives of the current study was to produce MSNs with increased specific surface area and pore volume and hence to achieve high loading of drug molecules (Slowing et al., 2008). The chosen SBA-16 nanoparticles presented high surface area and good pore volume prior to the loading studies. Passive loading was chosen as the preferred method to load the active molecules and to increase the loading efficiency. In this process

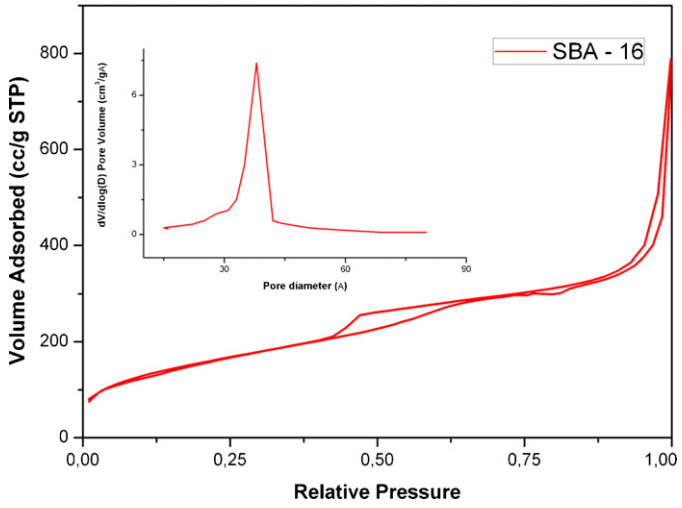

Fig. 3. Nitrogen adsorption isotherm for synthesized SBA-16. The inset image shows the pore size distribution.

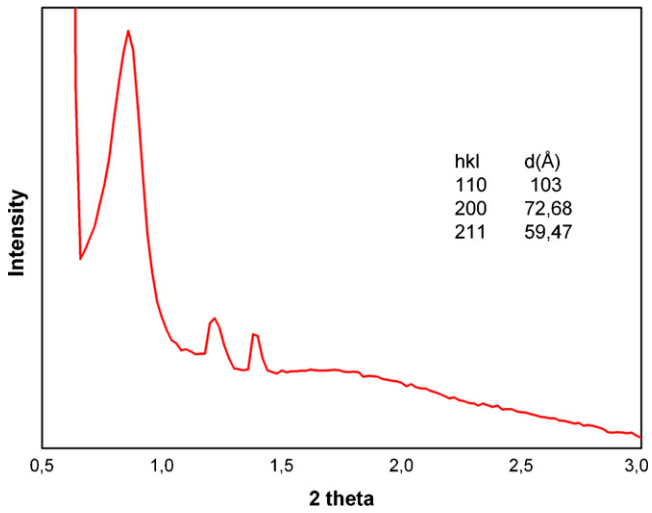

Fig. 4. Typical XRD pattern of SBA-16 materials.

a certain amount of SBA-16 nanoparticles is placed in a supersaturated organic solution of the active substance to facilitate drug adsorption. The active molecules are then diffused in the SBA-16 channel pores and onto the outer surface. SBA-16 pore dimensions are large enough to host the loaded material.

Among the influential features of the loading process is the polarity of the organic solvent. In some cases more polar solvents hamper the drug loading and essentially the whole process depends on the solvent properties (Charnay et al., 2004). In our studies CBZ was dissolved in methanol and OXC, RFN in DMF, respectively. Each solvent was selected in respect to the highest drug solubility in the appropriate solvent. OXC and RFN with $\log P = 1.76$ and $\log P = 7.5$, respectively, are slightly soluble in any solvent but DMF. Attempts to use acetone, methanol and dichloromethane showed negligible drug loading. Although CBZ ($\log P = 1.31$) is soluble in several organic solvents, methanol was proved the most suitable solvent due to the highest solubilisation capability.

The loading process revealed substantial drug loading (DL) efficiency for each active substance varying from 17 to 25% and a decreasing order of CBZ > RFN > OXC. In Table 1, CBZ showed high DL in less polar solvents in contrast to the other two drugs that achieved better DL in highly polar solvents.

3.3. Physicochemical characterisation

Fig. 5a and b shows the representative DSC thermograms of pure CBZ, TLP and RFN and drug loaded SBA-16, respectively. Carbamazepine exhibits enantiotropic polymorphism, which means a transition temperature can be observed below the melting point of either of the polymorphs at which both these forms have the same free energy. Above the transition temperature, the higher melting form (I) has the lower free energy and is more stable.

However the lower melting form III is more stable below the transition temperature since it has the lower free energy. The transition temperature of CBZ enantiotropic forms has been reported to be around 71 °C (Behme and Brooke, 1991). Hence, under ambient conditions form III is the most stable form. According to other

Table 1
Drug loading percentage ($n = 3$) of the three active substances with different $\log P$ values.

Drug	Drug loading (%)	Solvent	$\log P$
CBZ	25.2 ± 0.25	MeOH	1.31
OXC	17.38 ± 0.18	DMF	1.76
RFN	18.34 ± 0.34	DMF	7.50

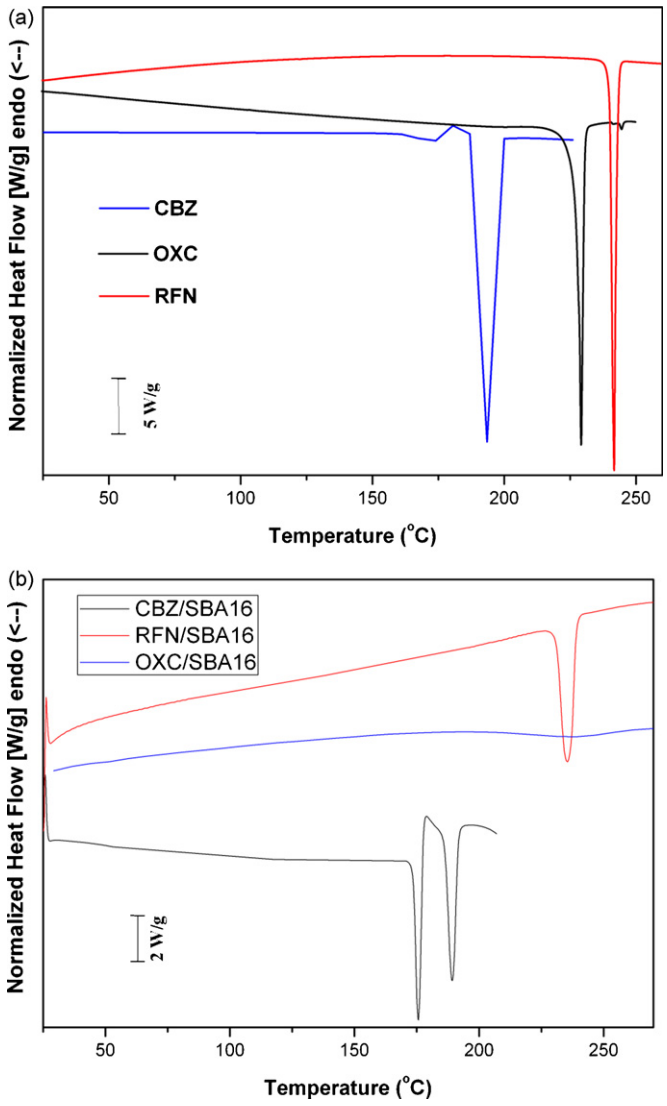

Fig. 5. DSC thermograms of (a) pure active substances and (b) drug loaded SBA-16 nanoparticles.

researchers (Katzhendler et al., 1998; Grzesiak et al., 2003) the DSC thermograms of CBZ form III shows two endotherms. The first endotherm is present in the range 170–175 °C and is not followed by any exothermic event while a sharp endotherm occurs at the range 189–192 °C.

Pure carbamazepine (Fig. 5a) showed a small melting endotherm at 175.98 °C followed by a second endotherm at 192.35 °C. These two endotherms correspond to form III and I of carbamazepine, respectively. The melting endotherm at 192.35 °C indicates that the used carbamazepine herein was form III. Oxcarbazepine showed a melting endotherm at 229.7 °C where no signs of occurrence of polymorphism have been observed up to date. The DSC studies of RFN revealed a melting endothermic peak at 241.9 °C.

The loaded SBA-16 thermogram of CBZ showed an increased endothermic peak at 175 °C (Fig. 5b) with a decrease in the enthalpy of form III at 192.35 °C. An increase of the enthalpy at 175 °C indicates transformation of form III to trigonal form II (Katzhendler et al., 1998) and the transition occurs by solid liquid transformation. The decrease of the second endothermic peak 192.35 °C suggests that part of form III was not converted to form II but only a fraction. This type of transformation is directly related to the solvent used for CBZ loading and could result substantial differences on the crystal and molecular structure (Lowes et al., 1987). On the

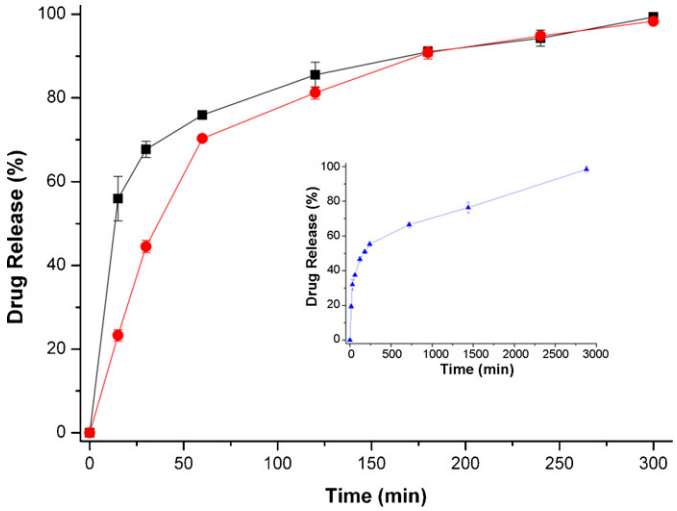

Fig. 6. Dissolution profiles of CBZ (■), OXC (●) and RFN (▲, inset) loaded SBA-16 nanoparticles ($n = 3$).

same reasoning OXC was found to be amorphous in the absence of an endothermic peak of the DSC thermogram. In contrast, RFN retained its crystalline structure and the RFN/SBA-16 thermogram showed a distinct endothermic peak at 235.3 °C. As it can be seen there is a shift from the melting point of the bulk RFN. This effect has been previously reported indicating the presence of RFN inside the pores of the silica nanoparticles (Riikonen et al., 2009). The melting of crystalline RFN inside the porous is observed at lower temperatures compared to the melting point of RFN outside the pores. This effect is due to the crystal size which inside the pores is restricted by the pore size. A decrease in the pore size results lower melting points of the active substance. This observation confirms the presence of crystalline RFN within the silica pores.

3.4. Dissolution studies

Dissolution profiles of SBA-16 loaded nanoparticles with CBZ, OXC and RFN were investigated in phosphate buffer dissolution medium. Accurately weighed amounts of the prepared samples were used under sink conditions ($C < 0.2Cs$). Interestingly as it shows in Fig. 6 rapid release patterns were observed for CBZ and OXC, respectively. In both cases the active substance was released in 5 h following almost identical profiles. In contrast, RFN displayed prolonged release patterns for 48 h. As it can be seen in Fig. 6 (inset) a burst release of RFN was observed in the first 3 h where 50% of the active was released. After the initial burst release, RFN exhibited slower release rate. This first order release mechanism has been also previously observed and it is related to drug diffusion process (Vallet-Regi et al., 2007). The inclusion of the three antiepileptic drugs within the silica nanoparticles resulted an efficient particle size reduction and hence improved dissolution rates. The above release profiles and the drug loading efficiency are of great interest for pharmaceutical application in order to improve the delivery of poorly soluble drugs by increasing absorption and bioavailability.

3.5. Cell cytotoxicity

Nowadays, nanomaterials are widely used in several biopharmaceutical applications and in many cases SiO_2 nanoparticles are considered to induce cytotoxicity in various cell culture lines (Lin et al., 2006). In the current study we carried out cytotoxicity studies using 3T3 cells. As a result the SBA-16 nanoparticles demonstrated very low cytotoxicity (Fig. 7) and the reduction of the fibroblast activity at concentrations higher than 800 μg/ml. Furthermore, the

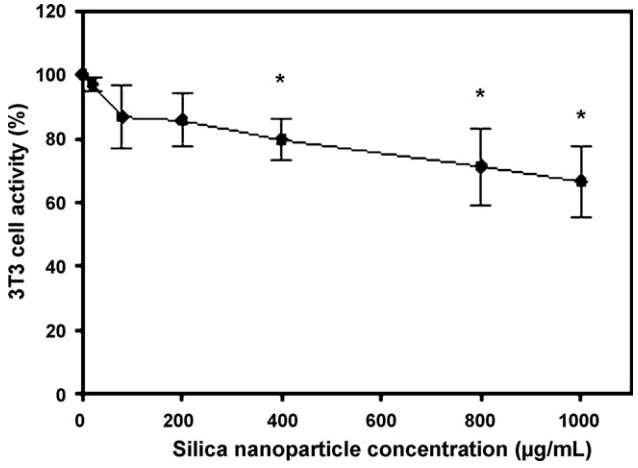

Fig. 7. Dose-dependent toxicity of silica nanoparticles on 3T3 cells (fibroblasts). 3T3 cells were treated with various concentrations of silica nanoparticles for 24 h. Cell viability was determined by MTT assay. Control cells cultured in absence of nanoparticles in parallel to the treated groups. Values were the mean ± SD from three independent experiments. Significance indicated by: $^{*}p < 0.05$ versus control cells.

cell activity did not decrease below 67% even after incubating the cells with 1 mg/ml of nanoparticles. This result agrees to the one reported by Napierska et al. (2009) who studied the effect of the size of silica nanoparticles on cell toxicity on human endothelial cells (EAHY926). According to the group findings, cell viability was reduced progressively as the nanoparticle size decreased. Our data coincide with those reported for the toxicity induced by particles of 104 nm. Cytotoxicity results indicate that SBA-16 could be effectively used as a platform for delivery of other active substances such as anticancer drugs.

4. Conclusions

In the present study we used synthesized SBA-16 nanoparticles with high surface area and cubic mesoporous structure for loading of three antiepileptic active substances. The results obtained showed that all drugs could be loaded with great efficiency into the SBA-16 and provide sustained release at least in the case of RFN. More importantly, cell culture studies 3T3 cell demonstrated very low cytotoxicity. Based on the above results, SBA-16 nanoparticles could be used as a model drug delivery carrier of various active substances.

References

Amidon, G.L., Löbenberg, R., 2000. Modern bioavailability, bioequivalence and biopharmaceutics classification system. New scientific approaches to international regulatory standards. Eur. J. Pharm. Biopharm. 50, 3–12.

Amidon, G.L., Lunnernas, H., Shah, V.P., Crison, J.R., 1995. A theoretical basis for a biopharmaceutic drug classification: the correlation of in vitro drug product dissolution and in vivo bioavailability. Pharm. Res. 12, 413–420.

Beck, J.S., Vartuli, J.C., Roth, W.J., Leonowicz, M.E., Kresge, C.T., Schmitt, K.D., Chu, C.T.-W., Olsen, D.H., Sheppard, E.W., McCullen, S.B., Higgins, J.B., Schlenker, J.L.J., 1992. A new family of mesoporous molecular sieves prepared with liquid crystal templates. J. Am. Chem. Soc. 114, 10834–10843.

Behme, R.J., Brooke, D., 1991. Heat of fusion measurement of a low melting polymorph of carbamazepine that undergoes multiple-phase changes during differential scanning calorimetry analysis. J. Pharm. Sci. 80, 986–990.

Blanco, E., Kessinger, C.W., Sumer, B.D., Gao, J., 2009. Multifunctional micellar nanomedicine for cancer therapy. Exp. Biol. Med. (Maywood) 234, 123–131.

Charnay, C., Begu, S., Tourne-Peteilh, C., Nicole, L., Lerner, D.A., Devoisselle, J.M., 2004. Inclusion of ibuprofen in mesoporous templated silica:drug loading and release property. Eur. J. Pharm. Biopharm. 57, 533–540.

Delehanty, J.B., Mattoussi, H., Medintz, I.L., 2009. Delivering quantum dots into cells: strategies, progress and remaining issues. Anal. Bioanal. Chem. 393, 1091–1105.

Douroumis, D., Fahr, A., 2006. Nano and micro-particulate formulations of poorly water soluble drugs by using a novel optimized technique. Eur. J. Pharm. Biopharm. 63, 173–175.

Douroumis, D., Fahr, A., 2007. Formulation and stabilization of Carbamazepine colloidal suspensions. Eur. J. Pharm. Sci. 30, 367–374.

Grzesiak, A.L., Lang, M., Kim, K., Adam, J., Matzger, A.J., 2003. Comparison of the four anhydrous polymorphs of carbamazepine and the crystal structure of form I. J. Pharm. Sci. 92, 2260–2271.

Heikkilä, T., Salonen, J., Tuura, J., Kumar, N., Salmi, T., Murzin, D.Y., Hamdy, M.S., Mul, G., Laitinen, L., Kaukonen, A.M., Hirvonen, J., Lehto, V.-P., 2007. Evaluation of mesoporous TCPSi, MCM-41, SBA-15, and TUD-1 materials as API carriers for oral drug delivery. Drug Deliv. 14, 337–347.

Huo, Q., Margoleses, S.I., Ciesla, U., Feng, U.P., Gier, D.E., Sieger, P., Leon, B.F.R., Petroff, P.M., Schuth, F., Stucky, G.D., 1994. Generalized synthesis of periodic surfactant/inorganic composite material. Nature 368, 317–320.

Katzhendler, I., Azouryb, Friedman, R.M., 1998. Crystalline properties of carbamazepine in sustained releasehydrophilic matrix tablets based on hydroxypropyl methylcellulose. J. Control. Release 54, 69–85.

Kortesuo, P., Ahola, M., Karlsson, S., Kangasniemi, I., Yli-Urpo, A., Kiesvaara, J., 1999. Silica xerogel as an implantable carrier for controlled drug delivery-evaluation of drug distribution and tissue effects after implantation. Biomaterials 21, 193–198.

Kresge, C.T., Leonowicz, M.E., Roth, W.J., Vartuli, J.C., Beck, J.S., 1992. Ordered mesoporous molecular sieves synthesized by a liquid-crystal template mechanism. Nature 359, 710–712.

Lin, W.S., Huang, Y.W., Zhou, X.D., Ma, Y.F., 2006. In vitro toxicity of silica nanoparticles in human lung cancer cells. Toxicol. Appl. Pharmacol. 217, 252–259.

Lin, W., Rieter, W.J., Taylor, K.M., 2009. Modular synthesis of functional nanoscale coordination polymers. Angew. Chem. Int. Ed. Engl. 48, 650–658.

Liong, M., Lu, J., Kovochich, M., Xia, T., Ruehm, S.G., Nel, A.E., Tamanoi, F., Zink, J.I., 2008. Multifunctional inorganic nanoparticles for imaging, targeting, and drug delivery. ACS Nano 2, 889–896.

Lowes, M.M.J., Caira, M.R., Lotter, A.P., Van Der Watt, J.G., 1987. Physicochemical properties and X-ray structural studies of the trigonal polymorph of carbamazepine. J. Pharm. Sci. 76, 744–752.

Mosmann, T., 1983. Rapid calorimetric assay for cellular growth and survival: application to proliferation and cytotoxicity assays. J. Immunol. Methods 65, 55–63.

Napierska, D., Thomassen, L.C.J., Rabolli, V., Lison, D., Gonzalez, L., Kirsch-Volders, M., Martens, J.A., Hoet, P.H., 2009. Size-dependent cytotoxicity of monodisperse silica nanoparticles in human endothelial cells. Small 5, 846–853.

Polyak, B., Friedman, G., 2009. Magnetic targeting for site-specific drug delivery: applications and clinical potential. Expert Opin. Drug Deliv. 6, 53–70.

Qu, F., Zhu, G., Huang, S., Li, S., Zhang, J.S.D., Qiu, S., 2006. Controlled release of Captopril by regulating the pore size and morphology of ordered mesoporous silica. Micropor. Mesopor. Mater. 92, 1–9.

Ravikovitch, P.I., Neimark, A.V., 2000. Relations between Structural parameters and adsorption characterization of templated nanoporous materials with cubic symmetry. Langmuir 16, 2419–2423.

Riikonen, J., Mäkilä, E., Salonen, J., Lehto, V.P., 2009. Determination of the physical state of drug molecules in mesoporous silicon with different surface chemistries. Langmuir 25, 6137–6142.

Schiffelers, R.M., Storm, G., 2008. Liposomal nanomedicines as anticancer therapeutics: beyond targeting tumor cells. Int. J. Pharm. 364, 258–264.

Slowing, I.I., Vivero-Escoto, J.L., Wu, C.W., Lin, V.S., 2008. Mesoporous silica nanoparticles as controlled release drug delivery and gene transfection carriers. Adv. Drug Deliv. Rev. 60, 1278–1288.

Sperling, R.A., Rivera, G.P., Zhang, F., Zanella, M., Parak, W.J., 2008. Biological applications of gold nanoparticles. Chem. Soc. Rev. 37, 1896–1908.

Vallet-Regi, M., Balas, F., Arcos, D., 2007. Mesoporous materials for drug delivery. Angew. Chem. Int. Ed. 46, 7548–7558.

Vallet-Regi, M., Ramila, A., del Real, R.P., Perez-Pariente, J., 2001. A new property of MCM-41: drug delivery system. Chem. Mater. 13, 308–311.

Wen, L.X., Ding, H.M., Wang, J.X., Chen, J.F., 2006. Porous hollow silica nanoparticles as carriers for controlled delivery of ibuprofen to small intestine. J. Nanosci. Nanotechnol. 9–10, 3139–3144.

Zhao, D., Huo, Q., Feng, J., Chmelka, B.F., Stucky, G.D., 1998. Nonionic triblock and star diblock copolymer and oligomeric surfactant syntheses of highly ordered, hydrothermally stable, mesoporous silica structures. J. Am. Chem. Soc. 120, 6024–6036.